UCRL-JC-130362
PREPRINT

Numerical Modeling of Porous Elastic-Viscoplastic Material with Tensile Failure

O. Yu. Vorobiev
L.A. Glenn

This paper was prepared for submittal to the
International Conference on Computational Engineering Science
Atlanta, GA
October 6-9, 1998

March 31, 1998

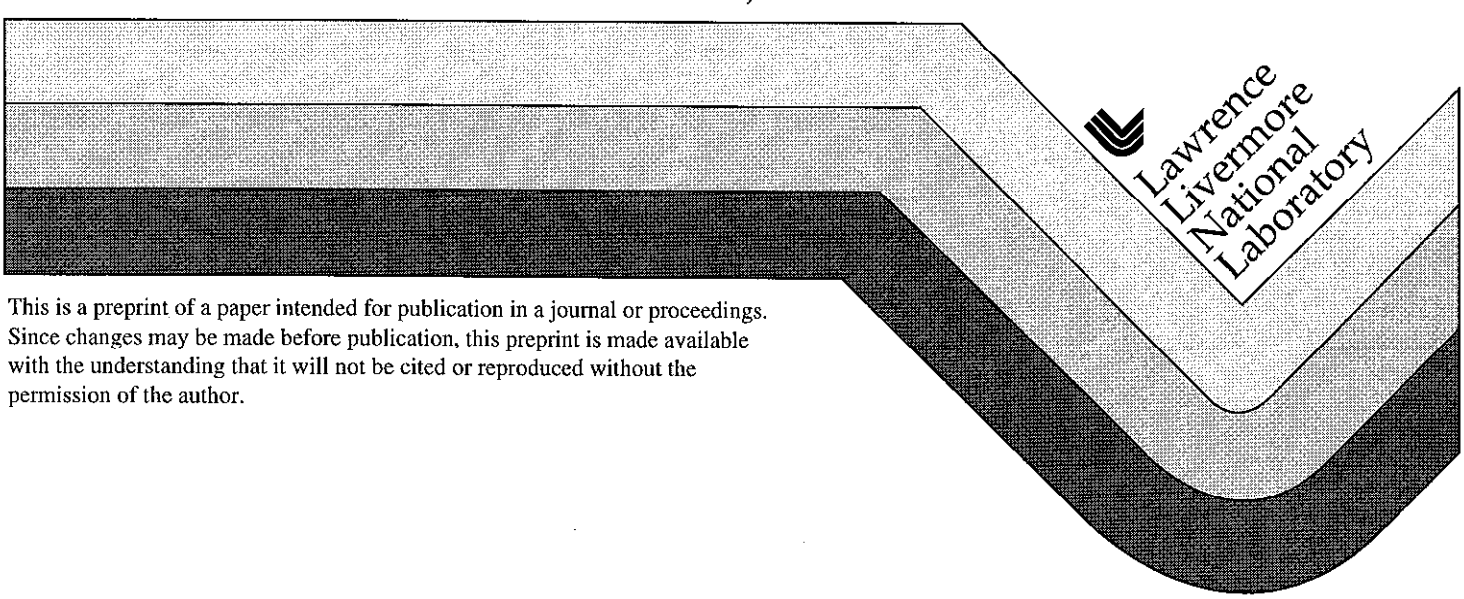

Numerical Modeling of Porous Elastic-Viscoplastic Material with Tensile Failure

OlegYu.Vorobiev
Lewis A. Glenn

Geophysics and Global Security Division
Lawrence Livermore National Laboratory
Livermore, CA 94550, USA

Summary

We report here on the development of a multi-material hydrocode for simulation of elastoplastic flows with large deformations. Using this hydrocode a new constitutive model for porous elastic-viscoplastic materials has been evaluated and the penetration of an aluminum projectile into porous rock material has been simulated numerically. The dependence of the penetration depth upon model parameters has been studed.

Introduction

In the present work, an alternative formulation of elastoplasticity is used, based on symmetric elastic distortional deformation tensor proposed in [1]. This tensor is referred to the present configuration and its usage implies isotropic response. Such an "alternative" formulation of plasticity has the conceptual advantage that there is no need to introduce both total and plastic deformation measures.

Constitutive equations

The mass and the momentum conservation laws for material α can be expressed as following:

$$\begin{aligned}
&\frac{\partial \rho_\alpha}{\partial t}+\frac{\partial \rho_\alpha u_x}{\partial x}+\frac{\partial \rho_\alpha u_y}{\partial y}=-\nu\left[\frac{\rho u_y}{y}\right];\\
&\frac{\partial \rho_\alpha u_x}{\partial t}+\frac{\partial\left(\rho_\alpha u_x^2-\sigma_{xx}\right)}{\partial x}+\frac{\partial\left(\rho_\alpha u_x u_y-\sigma_{xy}\right)}{\partial y}=\nu\left[\frac{\sigma_{xy}-\rho u_x u_y}{y}\right];\\
&\frac{\partial \rho_\alpha u_y}{\partial t}+\frac{\partial\left(\rho_\alpha u_y^2-\sigma_{yy}\right)}{\partial y}+\frac{\partial\left(\rho_\alpha u_x u_y-\sigma_{xy}\right)}{\partial x}=\nu\left[\frac{\sigma_{yy}-\sigma_{\theta\theta}-\rho u_y^2}{y}\right];
\end{aligned} \tag{1}$$

Here ρ_α is the density of the component α, σ is the average stress tensor and $\mathbf{u}$ is the mass velocity.
The case $\nu=0$ corresponds to that of plane symmetry and the case $\nu=1$ to axial symmetry; y is the radial direction and x is the axial direction . To describe elastic-plastic behavior, we use the following equation for the unimodular tensor of elastic distortional deformation [1].

$$\dot{\mathbf{B}}_\alpha=\mathbf{L}\mathbf{B}_\alpha+\mathbf{B}_\alpha\mathbf{L}^{\mathrm{T}}-\frac{2}{3}(\mathbf{D}\bullet\mathbf{I})\mathbf{B}_\alpha-\mathbf{A}_{\mathrm{p}}^{\alpha};\quad \mathbf{A}_{\mathrm{p}}^{\alpha}=\Gamma_p^{\alpha}\left[\mathbf{B}_\alpha-\frac{3\mathbf{I}}{\mathbf{B}_\alpha^{-1}\bullet\mathbf{I}}\right]; \tag{2}$$

Γ specifies the plastic response of the material and is taken to be a function of the von Mises effective stress and the yield strength. For rate-dependent response, we used the function proposed by Swegle and Grady [2].

If the elastic deformation tensor is known, the deviatoric stress can be calculated for every component as $\mathbf{T}_\alpha = G_\alpha J_\alpha^{-1}(1-\phi_\alpha)(\mathbf{B}_\alpha - \frac{1}{3}(\mathbf{B}_\alpha \bullet \mathbf{I}))$; where G is the shear modulas, $J_\alpha = \frac{\rho_{o\alpha}}{\rho_\alpha}\frac{1-\phi_\alpha}{1-\Phi_\alpha}$, and Φ_α and ϕ_α are respectively the reference and the current porosities for material α. Using $\mathbf{D}$ (the symmetric part of the velocity gradient tensor $\mathbf{L}$), the partial pressure P_α and the deviatoric stress for material α, the evolution equations for internal energy of the given material can be expressed as

$$\rho_\alpha \dot{\varepsilon}_\alpha = -\sigma_\alpha \bullet \mathbf{D} = -P_\alpha\left(\mathbf{D}\bullet\mathbf{I} - \frac{\dot{\phi}_\alpha}{1-\phi_\alpha}\right) + \mathbf{T}_\alpha \bullet \mathbf{D} \qquad (3)$$

Equations (1)-(3) together with the constitutive equation for porosity growth (described below) and equations of state to calculate pressure represent the full system to be solved.

Strength of material

The model used here is intended to apply to both metals and geological porous materials. The physical phenomena that influence the yield strength Y are accounted by assuming a simple multiplicative form with Y being given by

$$Y = Y_o F_1(\varepsilon_p) F_2(p) F_3(\Omega) F_4(\beta) F_5(\theta)\left[\frac{1-\phi}{1-\Phi}\right] \qquad (4)$$

The functions F in (4) represent hardening and softening effects due to plastic strain (F_1), pressure sensitivity (F_2), distortional deformation damage (F_3) and melting (F_5). The function F_4 is introduced to decribe the difference of the yield strength in tension compared with that in compression. In the calculations described below the functions F_2, F_3 and F_4 were equal to 1 for aluminum and the function F_1 was equal to 1 for rock material. A detailed description of these functions, with the specific values for each of the coefficients, can be found in [3].

Evolution of porosity

The model used in the calculations to describe the behavior of a porous, visco-plastic, material undergoing damage was developed in [3]. Here we neglect the details.

To describe the porosity increase due to distortional deformation, the following equations is used:

$$\dot{\phi} = (1-\phi)\left[\frac{m_d(\rho\theta\xi_d')}{\mathrm{Max}(p,p^*)}\right] H(\phi^*-\phi) \geq 0 \quad , \quad \text{for } \phi_{max} < \phi^* \text{ and } p > -p_d \, . \qquad (5)$$

where m_d, ϕ^* and p^* are material constants, p_d is a positive function to be specified , ϕ_{max} is the maximum value of porosity for all time and $\rho\theta\xi_d'$ is the rate of dissipation due to distortional deformation.

The evolution equation for porous compaction is given by

$$\begin{aligned}
&\dot{\phi} = 0 && \text{for } \phi_{max} \geq \phi^* \text{ and } -p_d \leq p < 0 \, , \\
&\dot{\phi} = -(1-\phi) < -\mathbf{D}\bullet\mathbf{I} > H(\phi-\phi^*_{min}) \leq 0 && \text{for } \phi_{max} \geq \phi^* \text{ and } 0 \leq p \leq p_c \, , \\
&\dot{\phi} = -\Gamma_c < \phi - \phi_c^* > H(-\mathbf{D}\bullet\mathbf{I}) \leq 0 && \text{for } \phi_{max} \geq \phi^* \text{ and } p > p_c \, , \qquad (6)
\end{aligned}$$

The functions ϕ_c^* and ϕ_{min}^* are defined by the expressions

$$\phi_c^* = \text{Max}\,[\phi_c^{**}\,,\,\phi^*]\,, \qquad \phi_{min}^* = \text{Max}\,[\phi_{min}\,,\,\phi^*] \qquad \text{for } \phi_{max} \geq \phi^*\,. \tag{7}$$

The functional form of ϕ_c^{**} is chosen in order to control the slope of the pressure- volume curve at the onset of compaction and is defined by

$$\phi_c^{**} = \Phi \exp\left[-\left\{\frac{c_1 + (1-c_1)\,F_6(\sigma_e, Y)}{c_2 J_c}\right\}\left\{\frac{1-\Phi}{\Phi}\right\} < \left\{\frac{J_c}{J}\right\}^{c_2} - 1 > \right],$$

$$F_6(\sigma_e, Y) = c_3\left[\sin\left\{\frac{\pi}{2}\,\text{Min}\,(1, \frac{\sigma_e}{Y})\right\}\right]^{c_4},$$

$$0 \leq c_1 \leq 1\,, \quad c_2 > 0\,, \qquad 0 \leq c_3 \leq 1\,, \quad c_4 > 1\,, \tag{8}$$

where c_1 and c_2 are material constants that controls the shape of the pressure curve during compaction. The function F_6 controls shear enhanced compaction and it is characterized by the material constants $\{c_3, c_4\}$. Specifically, for $c_3>0$, the value of ϕ_c^{**} decreases as deviatoric stress σ_e is increased. Also, since F_6 is taken to be a function of σ_e/Y it automatically incorporates the effects of hardening, pressure sensitivity, damage, Lode angle and porosity on shear enhanced compaction.

The evolution equation for porous dilation, when the pressure is more negative than $(-p_d)$ is given by

$$\dot{\phi} = \Gamma_d \exp(c_d\phi)\, H(\phi_d^* - \phi)\, H(\mathbf{D}\bullet\mathbf{I}) \geq 0 \qquad \text{for } p \leq -p_d\,. \tag{9}$$

where the Γ_d is taken to be a function of strain rate that is specified in the form

$$\Gamma_d = \Gamma_{d0}\left[1 + \left\{\frac{|\mathbf{D}\bullet\mathbf{I}|}{D_d}\right\}^n\right] \tag{10}$$

It is expected that the value of p_d will decrease towards zero as damage evolves. However, the value of p_d is required to remain positive. Thus, for example, p_d can be taken to have the simple form

$$p_d = [1 - c_5\, f(\omega)]\, p_{d0}\,, \qquad 0 \leq c_5 < 1\,, \tag{11}$$

where p_{d0} and c_5 are material constants and the function $f(\omega)$ is specified in [3].

In addition, a measure of damage ω due to porous compaction and dilation is defined by the evolution equation

$$\dot{\omega} = \frac{1}{\varepsilon_v}\,\frac{|\dot{\phi}|}{(1-\phi)}\, H(1-\omega)\,, \tag{12}$$

which is integrated subject to the condition that ω vanishes in the reference configuration. Also, the Heavyside function ensures that ω never is greater than unity.

Using a Mie-Gruneisen EOS, a functional form for ϕ_d^* can be specified by determining the value of ϕ associated with $p= -p_d$ such that

$$\phi_d^* = 1 - \frac{\frac{1-\Phi}{J} + \frac{p_d}{\rho_{s0} C_{s0}^2}}{1 - \frac{\gamma_{s0}\,\varepsilon}{C_{s0}^2}}\,, \tag{13}$$

where thermal effects have been included.

The evolution equations (5), (6), (9) and (11) introduce seven nonnegative constants { m_d, ϕ^*, p^*, Γ_c, p_c, c_d, ε_v } and five functions { ϕ_c^*, ϕ_{min}^*, ϕ_d^*, Γ_d, p_d }.

Numerical Algorithm

In the present work, a Godunov scheme is used to integrate the mass and momentum equations (1). To solve the evolution equations (2) for the elastic deformation tensor, the velocity gradient tensor and relevant history variables describing plasticity are used in each cell. A monotone Godunov scheme provides a smooth velocity and velocity gradient **D** which, when substituted into the evolution equation for the elastic deformation tensor, gives a robust algorithm for updating the deviatoric deformations and stresses. The deviatoric stresses in turn are used to solve a Riemann problem for the elastic material. To ensure stability we split the time step into several substeps when integrating the equations for internal energy and porosity evolution.Then new, updated pressure and deviatoric stresses are used in (3) after porosity recalculation in each substep.

We have chosen the volume-of-fluid (VOF) formulation to treat interfaces. This approach proved to be very robust for problems where high accuracy in interface tracking is required (for example, Rayleigh-Taylor or droplet splash simulations)[4]. One of the main advantages of the VOF approach in comparison with other interface tracking methods is that there is no need to explicitly specify the interface, which can be reconstructed each time step using the volume fraction field. This makes the VOF method relatively easy to use in 3D.

To simplify the logic of the interface reconstruction, a rectangular grid is used. Orthogonal grid structure is also convenient to approximate the velocity gradient tensor and derivatives required for the second order scheme.

More information about the detailes of the numerical algorithm can be found in [5]

Simulation Results

To validate the computer code for penetration problems, experiments [6] on steel projectile impact into an aluminum target were simulated using the Steinberg-Guinan rate independent strength model for both target and projectile material. The calculated crater size is close to experimental as it is seen from Fig.1. The results are shown for two different velocities of the 6 mm steel projectile:1.85 km/s and 7.62 km/s.

To see how the new constitutive model describes experimental data on uniform compression of porous rock material, and spall damage of metal in uniaxial expansion, eqs.6 and 9 were integrated numerically by a "driver" routine that used a specified velocity gradient evolution for one element. The results are shown in Fig.2(a,b).

Fig.3 shows simulation results for a 1km/s impact of a cylindrical aluminum projectile on 30% porous tuff . The length of the projectile was 1.8cm and the diameter was 0.8 cm. The results are shown 30 μs after the impact. Using an elastic-perfectly plastic model for the aluminum (Fig.3.b) produces a more deformed impactor compared to viscoplastic model results (Fig.3.a) and approximately the same penetration depth. Changing the constant responsible for porous compaction from 0.98 to 0.7 makes the porous compaction slower. As a consequence of that, the strength of the rock material is less and the penetration of the porous material is deeper, and there is more damage to projectile on the periphery (Fig.3.c)

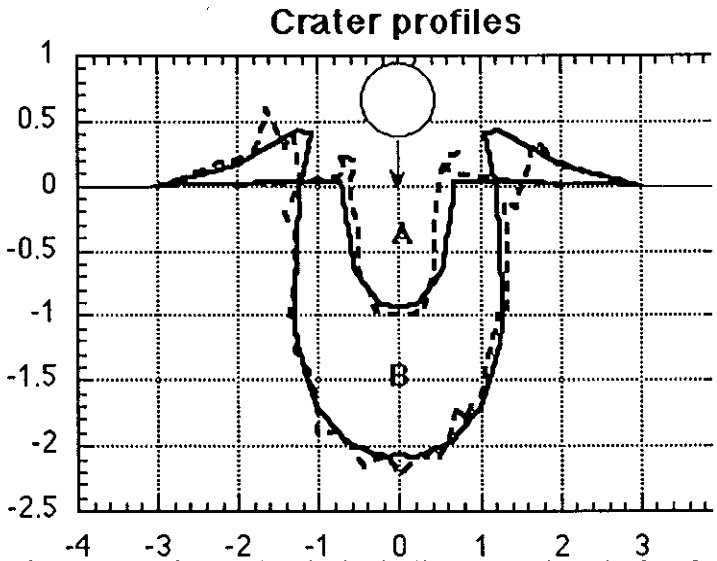

Fig.1 Experimental (dashed lines) and calculated crater profiles for different impact velocities of 6mm-diameter steel projectile: A-1.85 km/s, B-7.62 km/s

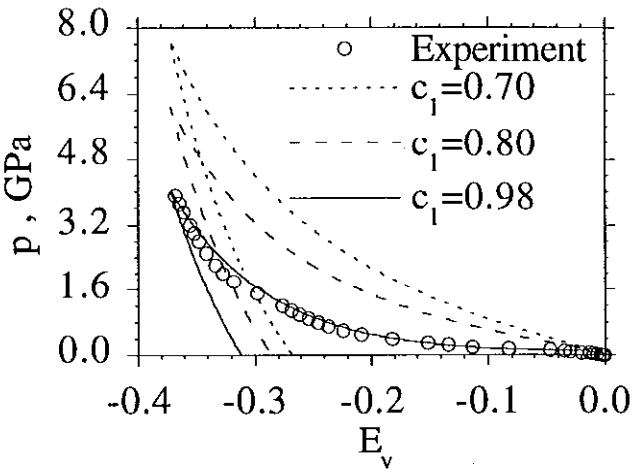

Fig.2(a) Comparison of the calculated compaction curve with experimental data [7] for Mt.Helen Tuff

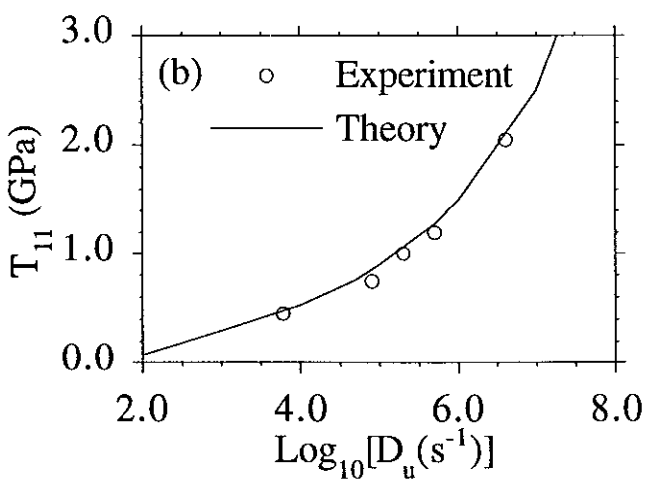

Fig.2(b)Comparison of the calculated (line) and experimental [8] (points) spall strength at different deformation rates

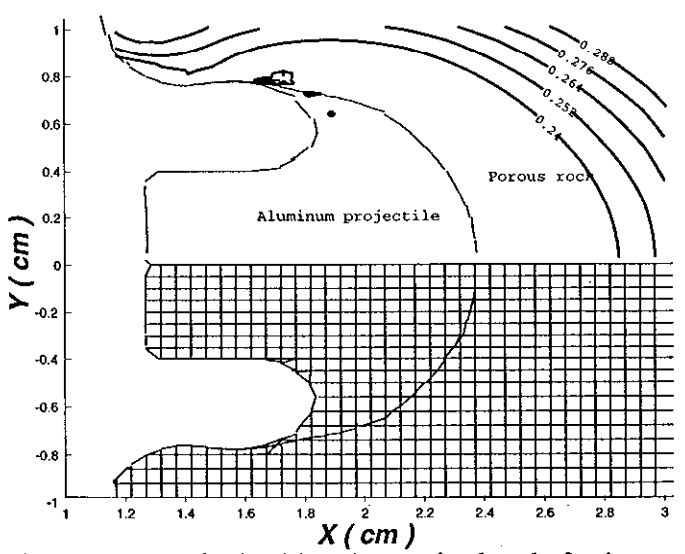

Fig.3(a) Numerical grid and porosity levels for impact of Al projectile on porous rock material. The viscoplastic model with hardening was used for Al.

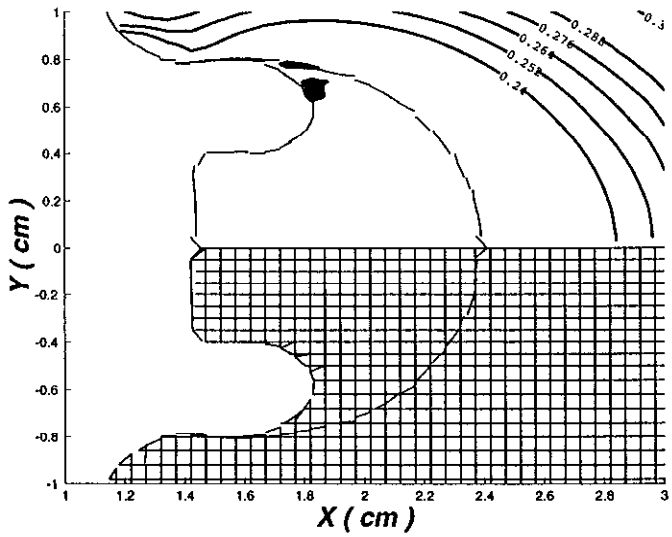

Fig.3(b) Numerical grid and porosity levels for impact of Al projectile on porous rock material.The elastic-perfectly-plastic model was used for Al.

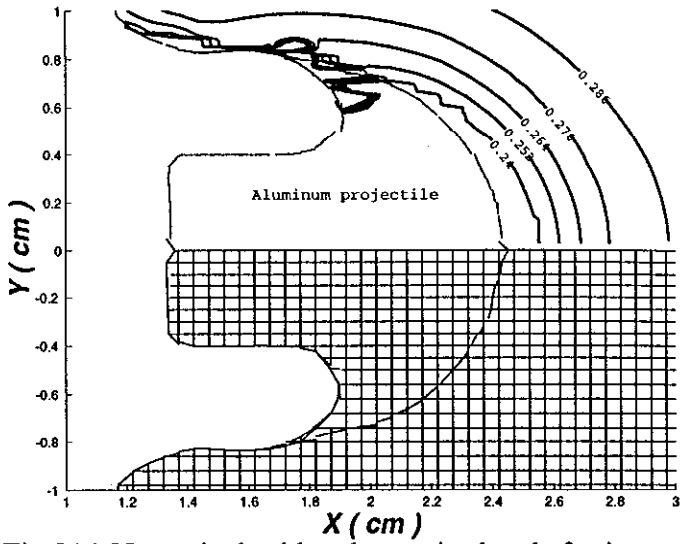

Fig.3(c) Numerical grid and porosity levels for impact of Al projectile on porous rock material.The value of c1 has been changed to be equal to 0.7 (instead of 0.98 used before)

References

1. Rubin, M. B., and Attia, A., (1996), "Calculation Of Hyperelastic Response Of Finitely Deformed Elastic-Viscoplastic Materials", Int. J. Numerical Meth. Engng., **39**, pp.309-320.

2. Swegle, J. W. and Grady, D. E., (1985), "Shock Viscosity And The Prediction Of Shock Wave Rise Times", J. Appl. Phys., **58**, p.692

3. Rubin, M.B., Vorobiev, O.Yu,Glenn, L.A., (1998) "Mechanical and Numerical Modeling of a Porous Elastic-Viscoplastic material with Tensile Failure", submitted to the International Journal of Solids and Structures

4. Puckett, E.G.; Almgren, A.S.; Bell, J.B.; Marcus, D.L.; and others, (1997), "A high-order projection method for tracking fluid interfaces in variable density incompressible flows", Journal of Computational Physics, **130**, (no.2),pp.269-82.

5. Vorobiev, O.Yu., Glenn, L. A (1998)" VGR-AStrength-Based Hydrocode with Automatic Mesh Refinement", Report LLNL, to be published

6. W.Harrison, C.Loupias, P.Outrebon and D.Turland (1995), "Experimental Data and Hydrocode Calculations for Hypervelocity Impact of Stainless Steel into Aluminum in the 2-8 km/s Range", Int.J.Impact Engng., Vol.17, pp.363-374

7. Heard, H. C., Bonner, B. P., Duba, A. G., Hock, R. N., and Stephens, D. R., (1973), "High Pressure Mechanical Properties Of Mt. Helen, Nevada, Tuff", Report LLNL No. UCID-16261

8. Kanel, G.I., Razorenov, S.V., Utkin, A.V., Baumung, K., Karow, H.U. and Licht, V., (1994). "Spallations Near The Ultimate Strength Of Solids", In High-Pressure Science and Technology-1993 (Eds. S.C. Schmidt, J.W. Shaner, G.A. Samara and M. Ross) American Institute of Physics Press, NY, pp.1043-1046.

*This work was performed under the auspices of the U.S. Department of Energy by Lawrence Livermore National Laboratory under contract No. W-7405-Eng-48.